Influence of Ge fraction on the properties of X and W-lines in SiGe: optical and first principles study

J. P. Leitão,[1,*] A. Carvalho,[1] N. M. Santos,[1,†] A. O. Ankiewicz,[1,‡] J. Coutinho,[1] N. A. Sobolev,[1] R. N. Pereira,[1] M. Barroso,[1] J. L. Hansen,[2] A. N. Larsen,[2] R. Jones,[3] and P. R. Briddon[4]

[1] *Departamento de Física, Instituto de Nanoestruturas, Nanomodelação e Nanofabricação, Universidade de Aveiro, Campus Universitário de Santiago, 3810-193 Aveiro, Portugal*
[2] *Institute of Physics and Astronomy, University of Aarhus, Aarhus, Denmark*
[3] *School of Physics, University of Exeter, Stocker Rd, EX4 4QL Exeter, UK*
[4] *School of Electrical, Electronic and Computer Engineering, University of Newcastle upon Tyne, Newcastle upon Tyne NE1 7RU, UK*

(Dated: February 25, 2011)

Photoluminescence and first principles calculations were used to investigate the electronic structure and stability of the W and X-lines in Si and SiGe alloys with low Ge content. The two optical centers were produced by irradiation with protons of 875 keV, in a fluency of 10^{16} H^+ cm^{-2}, of $Si_{1-x}Ge_x$ layers with $x = 0$, 0.69 and 1.25 at %. The influence of the Ge content is clearly different for both optical centers. The intensity of the W-line in photoluminescence was maximized for the annealing at 300°C for the three Ge fractions whereas a dependence on the Ge content was found for the X-line: 400°C for the Si layer and 450°C for the SiGe layers with $x = 0.69$ and 1.25 at %. For the W-line, with the increase of the Ge fraction, an absence of shift of the peak position was observed as well as a full width at half maximum broadening ratio of $d(\mathrm{FWHM})/dx = 229 \pm 48$ meV. For the X-line, a shift to higher energies was measured and a full width at half maximum broadening ratio of $d(\mathrm{FWHM})/dx = 543 \pm 134$ meV. Density functional calculations were performed in order to study the influence of the Ge content on electronic levels of the I_3 and I_4 centers proposed previously for the W and X-lines, respectively. A donor level close to the valence band was identified for both defects. In both cases, the donor level become more close to the valence band as the Ge fraction increases but the rate is much higher for the I_4 as compared to the I_3 defect. The thermal quenching of the intensity measured in photoluminescence for the W-line was interpreted as the release of the electron to a higher energy discrete level or to the conduction band. For the X-line, just the escape of the electron to the conduction band was identified. The activation energies in both centers were measured.

PACS numbers: 61.72.jj, 61.82.Fk, 71.15.-m, 71.55.-i, 71.55.-m

I. INTRODUCTION

The continued downscaling in silicon device fabrication requires the formation of ever shallower and more abrupt junctions with higher doping levels. Ion implantation and annealing are key steps for the introduction of dopants in silicon. Upon annealing, Si self-interstitials (I) resulting from implantation damage are prone to cluster as point-like defects or even extended defects, such as planar and rod-like {311} defects, and Frank dislocation loops.[1–3] Small interstitial clusters are observed before the nucleation of the rod-like {311} defects and dislocation loops.[4–8] Both interstitial clusters and extended defects can release Si self-interstitials, which are highly mobile even at room temperature[9,10] and are responsible for transient enhanced diffusion (TED) and deactivation of implanted dopants during the annealing.[2,11–16]

SiGe alloys provides one approach to the tailoring of physical parameters of silicon such as the electronic gap, effective mass and charge carrier mobility, simultaneously being compatible with the conventional Si technology.[17] SiGe alloys are particularly well-suited for operation in the cryogenic temperature and radiation-rich conditions typically found in space exploration.[18] In this kind of environment, radiation defects play a crucial role in the device performance. Another advantage of SiGe is the retardation of TED of boron which favors the downscaling of devices.[19,20] Additionally, it was observed a strong influence of the Ge fraction on the evolution of interstitial related defects.[3] For SiGe alloys with Ge content $\leqslant 5\%$ the formation and dissolution of rod-like {311} defects was observed whereas only dislocation loops are formed if the Ge content is $\geq 25\%$. Understanding the defects created in the matrix and their evolution during the subsequent annealing is crucial for the application of these diluted alloys in harsh environments.

Several self-interstitial related point defects in ion-implanted silicon have been detected by photoluminescence (PL). Depending both on the implantation parameters and the annealing temperature, several sharp and broad lines were observed.[4–8] These lines are related to clusters involving a different number of Si interstitials ranging from a small number to chains of I clusters and rod-like {311} extended defects. The W center, with a zero phonon line (ZPL) at 1018.2 meV, is created by particle irradiation or ion implantation of Si. Its intensity is maximized after an annealing at $\sim$ 300°C, and at $\sim$ 500°C is no longer observed.[21] As the intensity of the W-center diminishes another one, the X-center with a ZPL at 1039.8 meV, increases in intensity reaching the

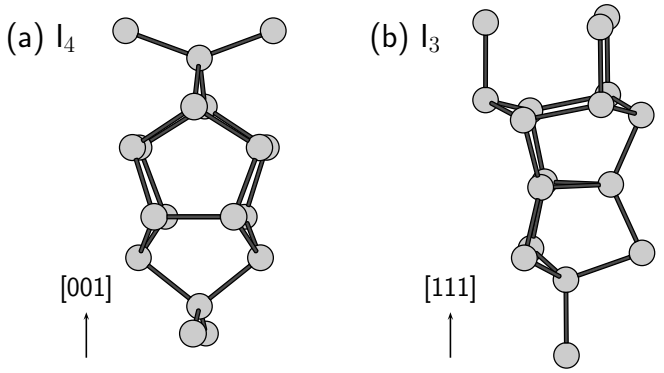

FIG. 1. Tetra-interstitial (a) and tri-interstitial (b) models for the X- and W- centers, respectively.

maximum for an annealing at ~ 450°C.[22–24] Both the W and X centers are of intrinsic nature.[25–27] Coomer et al[25,28] proposed that they originate respectively from a trigonal form of the tri-interstitial (I_3) and tetragonal tetra-interstitial (I_4) clusters.

The evidence in support of the tetra-interstitial model for the X-center [Fig. 1-a)] is quite strong. Initial stress-splitting studies suggested D_{2d} or T_d symmetry.[29] This is the same symmetry as that of the B3 EPR-center, which has been unambiguously related to I_4^+.[30–32] Under illumination with light of energy around 1.03 eV, another EPR center, NL51, with $S = 1$ has been detected,[33] suggesting the interpretation of the X-line as arising from the recombination of an exciton bound to a deep donor. Moreover, three phonon replicas of the X-line have been detected both in ^{nat}Si and ^{30}Si, showing that the defect has local vibrational modes above the Raman edge, characteristic of an interstitial defect.[27] These were very close to the highest vibrational frequencies of the I_4 defect, obtained from first-principles calculations.[34]

Regarding the I_3 model of the W-line, the situation is not so clear. The large stress parameters together with the moderate Huang-Rhys factor for the band imply a soft lattice in the locality of the center.[26] However, a phonon replica of the zero phonon line shows that the defect has a localized phonon mode at 70.0 meV and above the Raman frequency, characteristic of compressed bonds.[27] These points are consistent with Coomer's tri-interstitial model, consisting of a {111}-oriented three-member ring of Si interstitials, centered near the tetrahedral interstitial site [Fig. 1-b)].[25,34] However, this structure is now believed to be only metastable.[34,35] The most stable I_3 structure, 1.7 eV lower in energy, has C_2 symmetry and is electrically inert. Nevertheless, it is possible that other I_3 forms present in the material are not detected due to their lack of electrical or optical activity.

In spite of the intense research effort aimed at unraveling the structural properties and formation mechanisms of self-interstitial aggregates in silicon, the differences observed in SiGe alloys are still not well understood. In this work, we compare the optical properties and stability of the W- and X-lines in Si and SiGe alloys with low Ge content. In Sections II and III, the PL from a set of three samples in which a layer of $Si_{1-x}Ge_x$, grown by molecular beam epitaxy (MBE) on a Si substrate, for $x = 0$, 0.69 and 1.25 at % is described. In Sections IV and V, first-principles models of the I_3 and I_4 defects in SiGe alloys are used to find the shift of the donor level of these defects relative to Si. Experimental and theoretical results are discussed, highlighting the strengths and limitations of the models.

II. EXPERIMENTAL DETAILS

A Ge-free MBE Si layer (S layer) and two Ge-doped MBE Si layers ($Si_{0.9931}Ge_{0.0069}$ and $Si_{0.9875}Ge_{0.0125}$, denoted SG1 and SG2 layers, respectively) with a thickness of 3 μm were grown at 800°C on (001) Si substrates. The Ge content was determined by Rutherford back-scattering spectroscopy (RBS) using 1.5 MeV He^+ ions. Layers SG1 and SG2 were intentionally doped with Sb to be n-type. The concentration of conduction electrons measured by the capacitance-voltage technique amounted to 9×10^{15} cm^{-3} and 3×10^{15} cm^{-3} for SG1 and SG2 layers, respectively. These values should roughly correspond to the concentration of Sb donor atoms in the layers, given that the contamination resulting from unwanted compensating acceptor atoms in our MBE system should be lower than 10^{14} cm^{-3}. Although the S layer was not intentionally doped during growth, an n-type doping of about 3×10^{14} cm^{-3} resulted from the contamination of the growth chamber with Sb.

All samples were irradiated through a 10 μm thick Al foil with 875 keV protons (10^{16} H^+ cm^{-2}). The energy of the protons and the thickness of the Al foil were chosen based on a SRIM calculation[36] in order to place a broad profile of the damage (vacancies/interstitials) in the 3 μm thick SG layers. Using SRIM calculations, we estimate that the concentration maxima of 2×10^{21} cm^{-3} and 1.25×10^{20} cm^{-3} for the vacancies/interstitials and hydrogen atoms profiles, respectively, are located at 2.2 μm below the surface of the SG layers and have a full-width-at-half-maximum (FWHM) of about ~ 1 μm. It is noteworthy that the SRIM calculations are performed for 0 K, and at room temperature most of the vacancies and interstitials formed by the irradiation recombine. In moderately doped silicon, only about 1% of the vacancies/interstitials formed upon the irradiation should remain in the sample at room temperature.[37] Therefore, we estimate a maximum of the concentration profile of vacancies/interstitials after the irradiation at room temperature of about 2×10^{19} cm^{-3}, which is considerably lower than the maximum of the concentration profile of hydrogen atoms (1.25×10^{20} cm^{-3}). It should be mentioned that the maxima of the concentrations of vancancies/interstitials and of hydrogen atoms produced by the irradiations are several orders of magnitude higher than the concentration of Sb donors.

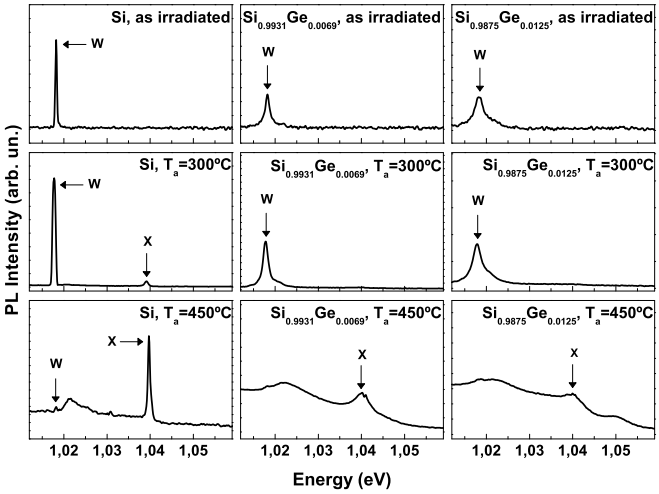

FIG. 2. PL spectra taken at 5 K for the Si, $Si_{0.9931}Ge_{0.0069}$ and $Si_{0.9875}Ge_{0.0125}$ layers as irradiated and, after the annealing at 300°C and after the annealing at 450°C. Both W and X-lines are identified in the spectra.

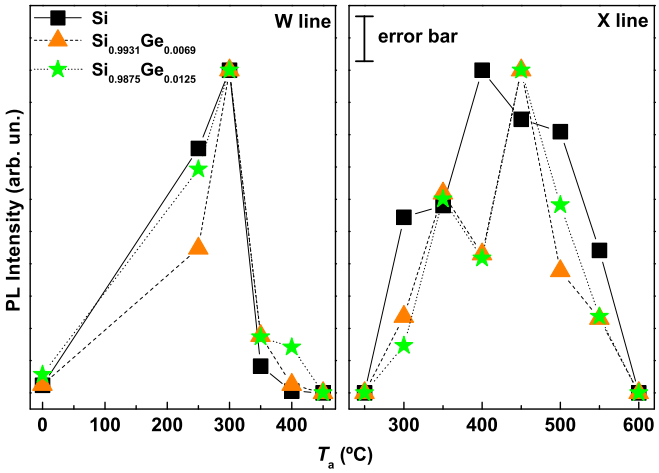

FIG. 3. Dependence on the annealing temperature of the X and W-lines intensities, taken at 5 K and for a laser power of 33 mW, for the proton irradiated Si, $Si_{0.9931}Ge_{0.0069}$ and $Si_{0.9875}Ge_{0.0125}$ layers. The intensities were normalized to the maximum value.

After irradiation the samples were annealed for 15 min in a N_2 atmosphere at temperatures between 100 and 650°C.

The PL measurements were made using a Bruker IFS 66v FTIR spectrometer equipped with a Ge diode detector. The samples were inserted in a helium gas flow cryostat which allowed the change of the temperature in the range $4 - 300$ K. The excitation source was the 488 nm line of an Ar^+ ion laser at a laser power of 13 or 33 mW measured in front of the cryostat window.

III. PL RESULTS

After the irradiation with 875 keV protons, the W-line at 1.0178 ± 0.0001 eV is observed in PL with a relative intensity that depends on the Ge content. The PL spectra for the as-irradiated S and SG layers are shown at the top of Fig. 2.

The annealing of the PL lines for S and SG layers was investigated in the temperature range $250 - 600$°C (see Fig. 3). The temperature dependence observed for the W-line is independent of the Ge content: the PL intensity reaches a maximum for 300°C, decreases for higher values and almost disappears for 450°C (see Fig. 2). With the increase of the Ge content, no shift of the peak position of the W-line is observed and the FWHM broadening rate is $d(\text{FWHM})/dx = 229 \pm 48$ meV. This value is close to the value of 191 meV, obtained by Tan et al[38].

The X-line starts to emerge for the annealing at 300°C at the expense of the W-line intensity, in accordance to previous studies.[22,23] The X-center clearly shows a different experimental behavior when compared to the W-center, with respect to its evolution with the Ge content. The annealing temperatures that maximizes the PL intensity are: 400°C for the S layer and 450°C for the SG layers. This result shows that the X-center will need more energy to stabilize in the alloy than in Si. This is compatible with the results of Crosby et al[3] in which the increase of the Ge content favors the formation of dislocation loops compared to the formation of {311} defects. With the increase of the Ge content, the X-line shifts to higher energy: 0.7 ± 0.2 meV and 2.2 ± 0.4 meV for SG1 and SG2 layers, respectively. At last, the broadening of the X-line occurs at a rate $d(\text{FWHM})/dx = 543 \pm 134$ meV, clearly higher than the observed for the W-line (see Fig. 2).

The difference in the influence of the Ge content on the positions of W and X-lines could be related to a higher localization of the wavefunctions of electron and hole on the center for the W-line as compared to the X-line.[21,39] In this way, the neighborhood of the center will be more important for the X-line than for the W-line which can justify the observed shift of the peak of intensity for just the X-line with the increase of the Ge content in the alloy and the higher value for the broadening rate of the FWHM for the X-center comparatively to the W-line. These experimental results support the previous attribution of the X-center to a cluster involving a larger number of self-interstitials than in the W-center.[28]

To study the influence of the Ge content on the non-radiative de-excitation mechanisms of the W and X-lines, we have chosen the annealing temperature that maximize the intensity of each center. For the study of the W-line, the three samples were annealed at 300°C, whereas for the study of the X-line, the S layer was annealed at 400°C and the SG layers at 450°C. The Arrhenius plots for the temperature dependence of the PL intensity of W-line are shown in Fig. 4. As the temperature increases, we observe a very small decrease of the PL intensity for $T \lesssim 30$ K and a strong quenching for higher values. For

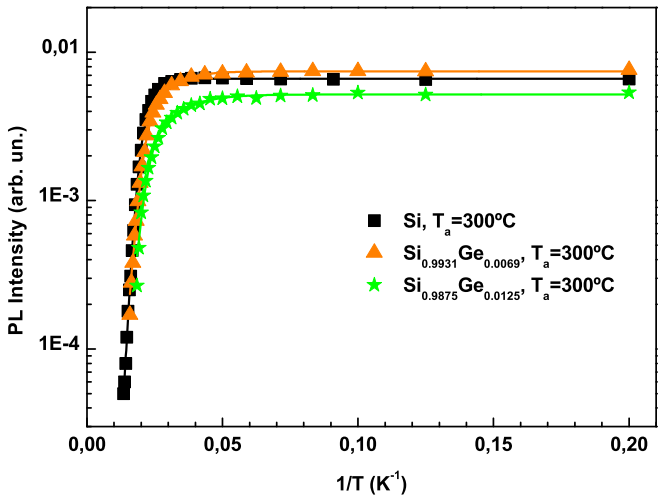

FIG. 4. Integral PL intensity dependence of the W-line in Si, $Si_{0.9931}Ge_{0.0069}$ and $Si_{0.9875}Ge_{0.0125}$ layers annealed at 300°C. The data points were fitted with Eq. 1 and the fitting parameters given in Table I.

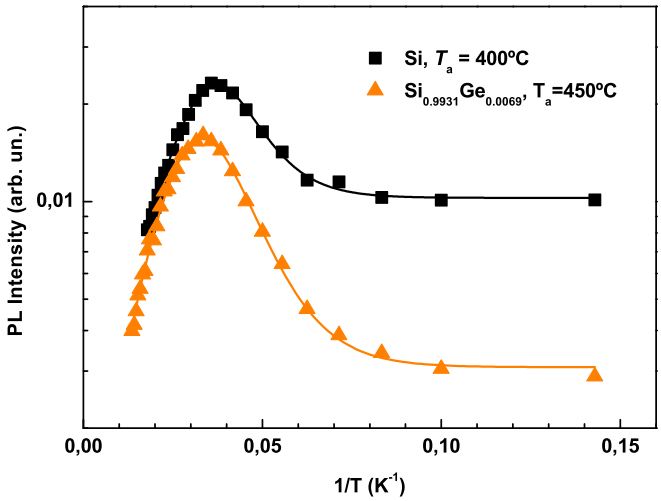

FIG. 5. Integral PL intensity dependence of the X-line in Si annealed at 400°C and in $Si_{0.9931}Ge_{0.0069}$ and $Si_{0.9875}Ge_{0.0125}$ layers annealed at 450°C, together with the respective fittings using Eq. 1 and the fitting parameters given in Table I.

the X-line, the broadening due to the increase of the Ge content (see Fig. 2) hindered this type of study for the SG2 layer. Hence, in Fig. 5 only the Arrhenius plots for the S and SG1 layers are shown. As the temperature is raised, it is observed an increase of the PL intensity for $T \lesssim 30\,\mathrm{K}$ and a strong decrease for higher values of T.

Under continuous excitation at low temperature, a thermodynamic equilibrium is established between free excitons in the excitonic band and excitons bounded to the defect. As the temperature of the sample is increased, this equilibrium is disturbed. The thermal decay of an exciton bounded to the center can occur through two different modes. In the first one, the exciton is released from the defect as a pseudo-particle to the excitonic band. The energy involved in the process is the localization energy of the exciton in the defect and corresponds to the difference between the excitonic band gap and the energy of the photon ($h\nu$) measured in the optical transition. In the second mode, just the carrier less bound to the defect is released. This carrier can go to one or more high energy discrete levels or directly to a band (conduction or valence band). The involved energy is the energy difference between the final and initial levels of the carrier in the transition. The energetic balance extracted from the temperature dependence of the PL intensity will contribute to the distinction between the two modes. As we will discuss ahead, the measured activation energies are not consistent with the first mode for both centers. Additionally, the first-principles modelling suggest the involvement for both centers of a deep donor which reinforce the above choice. In this way, we will proceed with the discussion in more detail of just the second mode, considering a system composed of a crystal with a donor and two charge carriers - electron, hole. Because our modeling results suggest that the defect is a donor, the less bound carrier is the electron.

A diagram with different energy levels of the system is presented in Fig. 6. In the ground state ($|D^0\rangle$), the system has the donor in a neutral state and no electrons or holes exist in the conduction and valence bands, respectively. The external excitation will promote the transition of electrons from the valence band to the conduction band ($|e^- + h^+\rangle$). These carriers can interact to form a free exciton in the excitonic band ($|fx\rangle$). Excitons bounded to the donor will exist in the radiative state ($|D^0 + bx\rangle$).

The release of the electron can occur to one or more high energy discrete levels or, alternatively, can occur to the conduction band. In this scope, a different number of high energy discrete levels and the involvement or not of the conduction band were considered in the discussion of the thermal quenching of the bound excitons for both W and X-centers. In the case of the W-line (Fig. 4), the best fit was obtained for a model that considers two channels for the escape of the electron: 1) to a high energy discrete level ($|D^+ + e^{-*}\rangle$) at an energy of E_1 from the radiative state of the donor; 2) to the conduction band ($|D^+ + e^-\rangle$) at an energy of E_2 ($E_2 > E_1$) from the radiative state.

For the X-line (Fig. 5), the experimental data show an increase of the PL intensity in the temperature range of $T \lesssim 30\,\mathrm{K}$. This behavior can be explained by the liberation of excitons or charge carriers bound to shallow traps through an energy of E_{nr} (see Fig. 6). As a consequence, the population of free excitons on the excitonic band will increase as well as the capture of some of them by the donor and the subsequent PL intensity. In this way, as we increase the temperature, two simultaneous processes occur: the thermal dissociation of the excitons bound to the donor and a feedback mechanism created by shallow traps. The best fit to the experimental data was obtained considering just one channel for the escape

of the electron: the carrier moves from the radiative state ($|D^0 + bx\rangle$) of the donor to the conduction band. To this transition corresponds the activation energy E_2 in the diagram of Fig. 6.

The general equation that describes the temperature dependance of the PL intensity is given by:[21]

$$I(T) = \frac{I_0}{\left[1 + c_1 \exp\left(-\frac{E_1}{kT}\right) + c_2\, T^{\frac{3}{2}} \exp\left(-\frac{E_2}{kT}\right)\right]\left[1 + \frac{g}{1 + b\, T^{\frac{3}{2}} \exp\left(-\frac{E_{nr}}{kT}\right)}\right]}, \quad (1)$$

where $I(T)$ is the PL intensity at temperature T and k is the Boltzmann constant. I_0 is a parameter related to the intensity at 0 K, $I(0) = I_0/(1+g)$. The expression in the first square brackets reflects the thermal equilibrium between the ground state and the first and second excited states of the system. Two de-excitation channels are represented inside these squared brackets: the escape of the electron to a higher energy discrete level by the second term and the escape of the electron to the conduction band by the third term. c_1 is proportional to the ratio between the degeneracy of the higher energy discrete level and the radiative state of the center whereas $c_2\, T^{\frac{3}{2}}$ includes the effective density of sates of the band, assuming that the probability of capturing an exciton at the donor is independent of temperature. The second square brackets describes the thermal supply of excitons from external shallow traps and g includes the temperature independent ratio of the trapping cross sections for excitons at the radiative defects and the competing shallow traps.

In Table I we show the parameters that characterize the best fits of Eq. 1 to the experimental data in Fig. 4 and Fig. 5. We must stress again that, for both centers, several models involving a different number of high energy discrete levels, and including or not transitions to the conduction band were considered, and the shown parameters are just for the best fit in each center. For the W-line, the channel involving the high energy discrete level is responsible for the small diminishing of the intensity in the range $T \leq 30$ K and activation energies of 28 ± 2, 11.7 ± 0.8 and 9 ± 1 meV were obtained for the S, SG1 and SG2 layers, respectively. For higher temperatures, the dominant de-excitation channel is the one involving the band which is responsible for the strong quenching of the PL. The fitted activation energies were 65 ± 6, 43 ± 3 and 40 ± 6 meV for the S, SG1 and SG2 layers, respectively. For both channels we observe that the increase of the Ge content results in the diminishing of the activation energies. This fact could be explained by an increase of the screening in the alloy comparing to the bulk Si which will become the levels more superficial. Facing the values obtained for the activation energies of both non-radiative channels, we can now justify the choice for the second mode of the thermal decay of the bound exciton. If the exciton is released as a whole, the activation energy for the strong quenching regime should be near to the value $E_g^{\mathrm{ex}} - h\nu \simeq 138$ meV. The obtained energies are clearly lower than this value which means that just the less bound carrier is released from the defect. For this center no increase of the intensity was observed with the increase of the temperature.

For the X-line, the raising of the temperature in the range $T \leq 30$ K showed an increase of the PL intensity

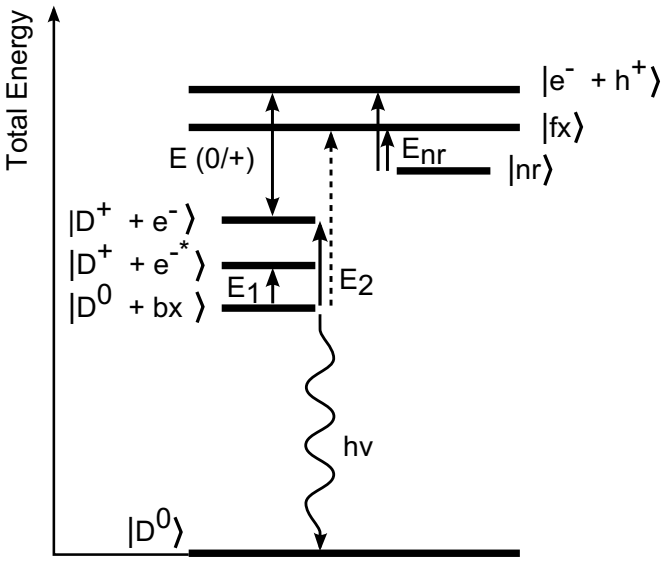

FIG. 6. Energy levels diagram illustrating the total energy of the system (crystal with a donor and two charge carriers — electron, hole). In the ground state ($|D^0\rangle$) of the system the donor is neutral and no electrons and holes exist in the conduction and valence bands, respectively. The energy $E(0/+)$ is the ionization energy of the donor. The radiative state of the defect ($|D^0 + bx\rangle$) corresponds to an exciton bound to a neutral donor. The excited state $|D^+ + e^{-*}\rangle$ is separated from the radiative state by E_1 and has the electron in a high energy discrete level and the hole bound to the donor. The state $|D^+ + e^-\rangle$ is separated from the radiative state by E_2 and the electron is in conduction band and the hole bound to the donor. In state $|e^- + h^+\rangle$ a free electron is in the conduction band and a free hole is in the valence band. The state $|fx\rangle$ corresponds to a free exciton. The state $|nr\rangle$ describes the presence of shallow traps that can supply excitons or charge carriers to the respective bands with the increase of the temperature. The dashed arrow corresponds to the release of an exciton as a whole from the donor to the excitonic band ($|fx\rangle$).

TABLE I. Fitting parameters of Eq. 1 to the data points obtained from the temperature dependence of the PL intensity for the W and X-lines measured for the Si, $Si_{0.9931}Ge_{0.0069}$ and $Si_{0.9875}Ge_{0.0125}$ layers.

W-line	$I_0 \times 10^{-5}$	c_1	E_1(meV)	c_2	E_2(meV)	g	b	$E_{\rm nr}$(meV)
Si	663 ± 1	800 ± 354	28 ± 2	49806 ± 54215	65 ± 6	0	0	0
$Si_{0.9931}Ge_{0.0069}$	744 ± 3	18 ± 5	11.7 ± 0.8	1348 ± 815	43 ± 3	0	0	0
$Si_{0.9875}Ge_{0.0125}$	519 ± 4	13 ± 5	9 ± 1	943 ± 1316	40 ± 6	0	0	0
X-line								
Si	18 ± 54	0	0	19 ± 14	14 ± 1	1777 ± 5268	514 ± 480	11 ± 1
$Si_{0.9931}Ge_{0.0069}$	1.2 ± 2.1	0	0	3.9 ± 0.9	12.5 ± 0.8	380 ± 674	236 ± 95	8.4 ± 0.7

parameterized by an activation energies E_{nr} of 11 ± 1 and 8.4 ± 0.7 meV for the S and SG1 layers. Such behavior was not observed for the W-line and this difference could be related to the type of defects, other than the W and X-defects, that are activated by the annealing at different temperatures. We must recall that the PL intensity of the W and X-centers is maximized at different temperatures: 300 and 400/450°C, respectively. For higher temperatures ($T > 30$ K), in the strong quenching regime of the PL, the activation energies of 14 ± 1 and 12.5 ± 0.8 meV for the S and SG1 layers, respectively, were obtained. The latter values support the interpretation that the thermal decay of the bound exciton is due to the escape of the less bound carrier. Again, it is observed through the small reduction of the activation energy, the same effect that with the increase of the Ge content in the alloy the electronic levels move in the direction of the bands. Finally, the activation energies are lower than the ones obtained for the same regime of strong quenching of the PL for the W-line and they are close to the free exciton dissociation energy in silicon (14.7 meV).[40]

The above PL results show clear differences in the electronic structure of both centers. First, for the W-line, both the transitions of electrons from the ground state to a high energy discrete level and to the conduction band have to be considered, whereas for the X-line there is no evidence for the first mechanism. Second, the radiative recombination of excitons at the X-center is partially fed by an external exciton traps.

The measured activation energies E_2 are consistent with the interpretation that the centers are deep donors, where the hole is more strongly bound than the electron (section V). According to this model, as illustrated in Fig. 6, for each center $E_g \simeq h\nu + E_2 + E(0/+)$, where $E(0/+)$ is the position of the donor level relative to the valence band.

IV. THEORETICAL METHOD

In order to establish a link between the experimental observations and the defect structure, we investigated the evolution of the electronic levels of the two interstitial models, previously proposed for the W- and X-centers in Si, in SiGe alloys using first-principles modeling. These are respectively a trigonal form of I_3 and I_4. The defects were modeled within the framework of density-functional theory. Core states were dealt with by using the pseudopotentials proposed by Hartwigsen, Goedecker and Hutter (HGH).[41] We adopted the local density approximation (LDA) for the exchange and correlation energy, together with an expansion of the Kohn-Sham states in a basis set of localized Cartesian Gaussian orbitals (CGOs), as implemented in the AIMPRO code.[42] For silicon, we used a contracted basis set with polarization functions to account for higher order momentum components, with a total of 13 functions per atom (44G*), as described in Ref. 47. The geometry, relative energies and electronic levels of the I_3 and I_4 defects in silicon calculated using this methodology are in close agreement with those that we have obtained previously using an uncontracted basis set of 28 functions per atom.[34] For germanium, we used an uncontracted basis set of $(4, 4, 2)$ (s, p, d) CGOs, with a total of 28 functions per atom.

Defects are placed in 216 atom cubic supercells, and the Brillouin zone (BZ) was sampled with the MP-2^3 special **k**-point sampling scheme of Monkhorst and Pack.[43]

The alloy was modeled by generating a series of random $Si_{216-n}Ge_n$ supercells. In accordance with the layers studied in PL in this work, the theoretical study was restricted to germanium concentrations below 2.5%, which corresponds to values of n between 0 and 5. For each n, we generated 20 SiGe supercells by placing the germanium atoms in random positions of the silicon lattice. The lattice parameter for the alloys was linearly interpolated between the calculated values for bulk Si and bulk Ge. In previous work it was shown that the calculated lattice parameters reproduce well the structural properties of the alloys over all the concentration range[44] and that, for such small concentrations, Vegard's law is still a good approximation.[45]

V. MODELING RESULTS

A. Defect structure and stability

The structure and stability of I_3 and I_4 in silicon have been described in a previous paper.[34] While I_4 is a very

stable defect with only one known low formation energy configuration, I_3 is very mobile[35] and the Coomer's form, which has been linked with the W center, is at least 1.6 eV higher in energy than the most stable configuration.[34] Here, we compare the behavior of the tetra-interstitial and Coomer's tri-interstitial in SiGe alloys having in view a discussion of the respective models for the W and X lines.[46]

The presence of the interstitial aggregate originates a compressive strain in the bonds of the surrounding lattice. In silicon, the bonds at the core of the defects are shortened, up to 15.5 and 10.4 % less than the bulk value for I_3 and I_4, respectively. As Ge atoms have a larger effective radius than Si, the binding energy between these interstitial clusters and Ge is negative or nearly zero, i.e., the lowest energy position for the Ge atom is at infinite distance from the I_3 and I_4defects, and the interstitial aggregates will prefer to form in Si-rich regions.

The shift of the radiative recombination energy $h\nu$ in SiGe alloys is due to the variation of the position of the energy level of the excitonic state ($|D^0 + bx\rangle$ in the diagram of Fig. 6) with the Ge concentration. It is related to long-range interaction between the Ge atoms at the SiGe host matrix and the defect, for example through the changes to the lattice parameter and band structure.

In order to quantify this effect, we have generated a series of 20 $Si_{216-n}Ge_n$:D supercells, where D stands for I_3 or I_4, with a total of 216+3 or 216+4 atoms, respectively. In order to isolate the long-range contribution, Ge atoms were not placed in the immediate neighborhood to the defects. All the other lattice positions were assumed to be equally probable. For each configuration, the positions of all the atoms were relaxed at a fixed volume, using the average equilibrium volume $V(x)$, where x is the Ge content in the alloy.

The defect formation energies are given by

$$E_f^D(x) = E_x(D) - E_x(S) - m\mu_{\rm Si}, \qquad (2)$$

where $E_x(D)$ is the average energy of the defective supercells with a Ge fraction x, $E_x(S)$ is the average energy of the bulk supercells for the same x, m is the number of self-interstitials and $\mu_{\rm Si}$ is the chemical potential for Si. It is interesting that the formation energies, calculated for a $\mu_{\rm Si}$ taken from bulk Si, remain practically constant with x (Fig. 7), even though the cohesive energy of silicon is higher. Thus, it is not surprising that the temperature range of stability of the defects varies little from Si to SiGe.

B. Ionization levels

The ionization energy, given relative to an arbitrary reference, can be obtained from the absolute difference between the total energies of supercells containing the defect D in the neutral and positive charge states,

$$\phi^D(0/+) = |E(\mathrm{D}^0) - E(\mathrm{D}^+)|. \qquad (3)$$

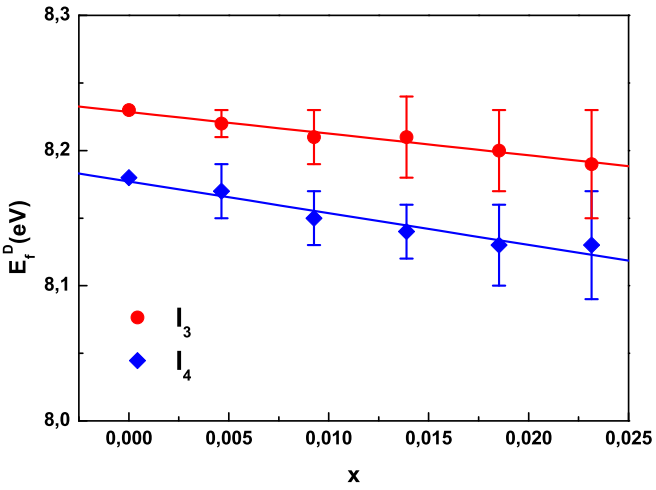

FIG. 7. Calculated formation energies of I_4 and Coomer's I_3 in $Si_{1-x}Ge_x$ alloys. $\mu_{\rm Si}$ was taken from bulk Si. Error-bars represent the statistical standard deviation of E_f for the configurations sampled.

The calculated ionization energies of the I_3 and I_4 defects are shown in Fig. 8. The energy $E(0/+)$ (Fig. 6) can be calculated by comparing the ionization energies of the defects, as a function of x, with the ionization energies of bulk (B) $Si_{216-n}Ge_n$ supercells:

$$E(0/+) = E_v + \phi^D(0/+) - \phi^B(0/+). \qquad (4)$$

This is equivalent to the marker method, using bulk as marker.[47] We have also shown for well-known defects that the marker method can be applied across a concentration range, yielding the shift of the defect levels with the germanium content.[48] A similar method can be used to compute elecron affinities. However, no acceptor level in the gap is found for I_3 nor I_4.

Since, as exposed in Section I, the assignment of the X-center to I_4 has been more firmly established, let us start by comparing the theoretical and experimental results for this defect. Using Eqs. 3 and 4, we obtain for I_4, $E(0/+) = 0.29 - (0.52 \pm 0.02)x$. The I_4 level does not move upwards at the same rate as the valence band, thus merging into its direction. Here, the uncertainty was estimated from the standard deviations of the total energies for the configurations sampled. Following the electron release model schematized in Fig. 6, the donor level of the X-center is at $E_v + E(0/+) = E_g - h\nu - E_2$. Comparing the calculated $E(0/+)$ for $x = 0$ with the value obtained from the measured quantities, $h\nu = 1.0398$ eV and $E_2 = 14$ meV, or $E(0/+) = E_v + 0.10$ eV, we notice that $E(0/+)$ is overestimated. The error (< 0.2 eV) is typical from this type of calculations (see Ref.48). However, this systematic error is not expected to affect our conclusions for SiGe alloys, since the interaction of the defect with germanium atoms in the dilute alloy can be viewed as a weak perturbation to the $x = 0$ system, and therefore improved accuracy can be expected when calculating the small shifts of the levels by comparison of

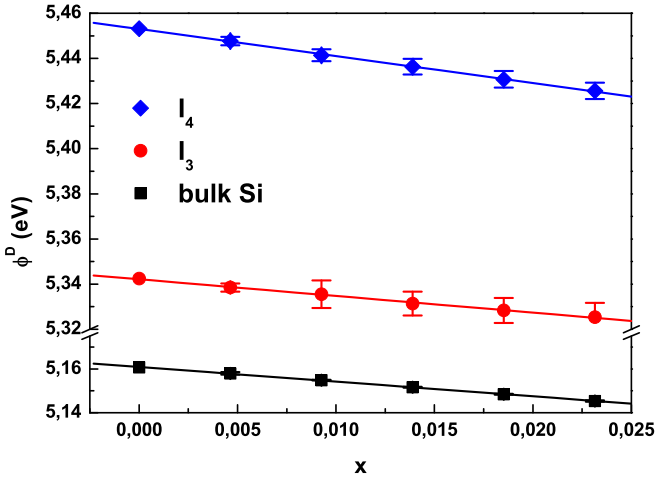

FIG. 8. Calculated ionization energies of the I_4 and Coomer's I_3 in $Si_{1-x}Ge_x$ alloys.

systems with different concentrations.

The variation of the photon energy can be estimated as

$$\frac{d\,(h\nu)}{dx} \simeq \frac{dE_g}{dx} - \frac{d}{dx}E(0/+) - \frac{d}{dx}E_2, \qquad (5)$$

where the bandgap energy is, for small x, given by $E_g = 1.155 - 0.43x$ eV .[49] The term most difficult to estimate is $\frac{d}{dx}E_2$, since the values measured for both concentrations are similar within the error bar. The contribution of the first two terms is $\frac{dE_g}{dx} - \frac{d}{dx}E(0/+) \simeq +0.09$ eV. The above shift gives 0.6 and 1.1 meV for $x = 0.0069$ and $x = 0.0125$, respectively. The first value matches the experimental shift of $h\nu$, while the second one is slightly less than the measured value, possibly due to the contribution $-\frac{d}{dx}E_2$. Hence, the theoretical and experimental results are consistent and their comparison suggests that $\frac{d}{dx}E_2$ is small.

For Coomer's I_3 model, we note that the behavior of the level is qualitatively different, as its distance from the valence band practically does not change [$E(0/+) = 0.18 - (0.07 \pm 0.02)x$]. First, we note that according to this model the level of I_3 is closer to the valence band than that of I_4. This would imply a higher photon energy in the radiative transition than for the I_4 center, in contrast with the peak energies measured experimentally (see section III) for the W and X-centers. Even thought the two defects have some resemblance, this error is acceptable within the expected error.

Regarding the variation of the recombination energy with x, we note that in this case the contribution $\frac{dE_g}{dx} - \frac{d}{dx}E(0/+)$ obtained from the I_3 model is in this case negative and large ($-0.36x$ eV). However, experimentally, a shift of $h\nu$ is not observed. The two results are not necessarily incompatible, if we note that experimentally E_2 in this case is larger than the values for the X-line and shows a clear decrease with x. Thus, the two terms may actually cancel. In contrast, this result gives additional evidence that the loss of excitons from the W center cannot take place through the release of the exciton as a whole. Since the variation of the free exciton binding energy is very small in SiGe (about $-0.01x$ eV[40]), that de-excitation mechanism would yield $\frac{d(h\nu)}{dx} \simeq \frac{dE_g}{dx} - \frac{d}{dx}E(0/+)$, making the I_3 model incompatible with experiment. nao sei se enetendi esta frase: se a desexcitacao do W for pela libertacao do excitao como um todo existe desacordo com a experiencia no que respeita a dependencia da energia do fotao com a fraccao de Ge, x? talvez se possa reescrever para ficar mais claro.

VI. CONCLUSIONS

In this work we present a thorough study of the optical properties and stability of the W and X-lines in Si and SiGe alloys with low Ge content ($x = 0.69, 1.25$ at %) through a complementary study of PL measurements and density functional calculations. The defects were produced by proton irradiation and subsequent annealing. An independence of the Ge content was found for the maximization of the PL intensity of the W-line (300°C) whereas for the X-line the presence of Ge shifted that temperature from 400°C (Si) to 450°C (SiGe alloys). We have compared the PL energy and de-excitation mechanisms of the W- and X-centers in Si and SiGe alloys, pointing out differences between the two centers. With increasing Ge content, no shift of the peak position of the W-line was observed while for the X-line a shift to higher energies was registered. Further, the FWHM broadening rates [d(FWHM)/dx] of both lines are quite different: 229 ± 48 meV for the W-line and 543 ± 134 meV for the X-line. Finally, although the thermal de-excitation of both centers can be described by the release of the weakly bound electron to a donor state, the activation energies and temperature dependence of the intensity of the two lines is different. Two non radiative de-excitation channels were identified for the W-line, one involving a high energy discrete level and the other involving the conduction band, whereas for the X-line there is experimental evidence for just the presence of the last one.

Self-interstitial cluster models (I_3 and I_4 for the W- and X-centers, respectively) were used to give additional insight into the influence of the presence of Ge. Using density functional calculations, we find that the position of the donor levels of I_3 and I_4 becomes closer to the valence band edge as the Ge concentration increases, however at very different rates: $\frac{d}{dx}E(0/+) = -0.07 \pm 0.02$ eV for I_3, but $\frac{d}{dx}E(0/+) = -0.52 \pm 0.02$ eV for I_4. These are found to be consistent with experiment if the radiative transition corresponds to a recombination of a weakly bound electron with a strongly donor-bound hole and the measured activation energy of the respective de-excitation process. However, a de-excitation process where the exciton is released as a whole is not compatible with the relation between the measured energies and the calculated shift of the donor level of the I_3 model.

* joaquim.leitao@ua.pt
† Present address: INOV-Inesc Inovação, Rua Alves Redol, 9, 1000-029 Lisboa, Portugal
‡ Present address: Continental Ausbildung Frankfurt am Main, Guerickestraße 7, 60488 Frankfurt am Main, Germany

[1] K. S. Jones, S. Prussin, and E. R. Weber, Appl. Phys. A: Materials Science & Processing **45**, 1 (1988).
[2] S. C. Jain, W. Schoenmaker, R. Lindsay, P. A. Stolk, S. Decoutere, M. Willander, and H. E. Maes, J Appl. Phys. **91**, 8919 (2002).
[3] R. T. Crosby, K. S. Jones, M. E. Law, A. N. Larsen, and J. L. Hansen, Mater. Sci. Semicond. Process. **6**, 205 (2003).
[4] J. L. Benton, S. Libertino, P. Kringhøoj, D. J. Eaglesham, J. M. Poate, and S. Coffa, J. Appl. Phys. **82**, 120 (1997).
[5] D. C. Schmidt, B. G. Svensson, M. Seibt, C. Jagadish, and G. Davies, J. Appl. Phys. **88**, 2309 (2000).
[6] S. Libertino, S. Coffa, and J. L. Benton, Phys. Rev. B **63**, 195206 (2001).
[7] M. Nakamura and S. Murakami, J. Appl. Phys. **94**, 3075 (2003).
[8] P. K. Giri, Semicond. Sci. Technol. **20**, 638 (2005).
[9] G. D. Watkins, Phys. Rev. B **12**, 5824 (1975).
[10] E. J. H. Collart, K. Weemers, N. E. B. Cowern, J. Politiek, P. H. L. Bancken, J. G. M. van Berkum, and D. J. Gravesteijn, Nucl. Instrum. Methods Phys. Res. B **139**, 98 (1998).
[11] P. M. Fahey, P. B. Griffin, and J. D. Plummer, Rev. Mod. Phys. **61**, 289 (1989).
[12] N. E. B. Cowern, K. T. F. Janssen, and H. F. F. Jos, J. Appl. Phys. **68**, 6191 (1990).
[13] P. A. Stolk, D. J. Eaglesham, H.-J. Gossmann, and J. M. Poate, Appl. Phys. Lett. **66**, 1370 (1995).
[14] P. A. Stolk, H.-J. Gossmann, D. J. Eaglesham, D. C. Jacobson, C. S. Rafferty, G. H. Gilmer, M. Jaraíz, J. M. Poate, H. S. Luftman, and T. E. Haynes, J. Appl. Phys. **81**, 6031 (1997).
[15] A. Ural, P. B. Griffin, and J. D. Plummer, J. Appl. Phys. **85**, 6440 (1999).
[16] N. E. B. Cowern, G. Mannino, P. A. Stolk, F. Roozeboom, H. G. A. Huizing, J. G. M. van Berkum, F. Cristiano, A. Claverie, and M. Jaraíz, Phys. Rev. Lett. **82**, 4460 (1999).
[17] F. Schäffler, Semicond. Sci. Technol. **12**, 1515 (1997).
[18] J. D. Cressler, Proc. IEEE **93**, 1559 (2005).
[19] P. Kuo, J. L. Hoyt, J. F. Gibbons, J. E. Turner, and D. Lefforge, Appl. Phys. Lett. **66**, 580 (1995).
[20] C. C. Wang, Y. M. Sheu, Sally Liu, R. Duffy, A. Heringa, N. E. B. Cowern, and P. B. Griffin, Mater. Sci. Eng., B **124-125**, 39 (2005).
[21] G. Davies, Phys. Rep. **176**, 83 (1989) and references therein.
[22] K. Terashima, T. Ikarashi, M. Watanabe, and T. Kitano, Mater. Sci. Forum **258&263**, 587 (1997).
[23] O. O. Awadelkelkarim, A. Henry, B. Monemar, J. L. Lindström, Y. Zhang, and J. W. Corbett, Phys. Rev. B **42**, 5635 (1990).
[24] A. O. Ankiewicz, N. A. Sobolev, J. P. Leito, M. C. Carmo, R. N. Pereira, J. L. Hansen, A. N. Larsen, Nucl. Instrum. Methods B **248**, 127 (2006).
[25] B. J. Coomer, J. P. Goss, R. Jones, S Oberg, and P. R. Briddon, Physica B **273/274**, 505 (1999).
[26] G. Davies, E. C. Lightowlers, and Z. E. Ciechanowska, J. Phys. C: Solid State Phys. **20**, 191 (1987).
[27] S. Hayama, G. Davies and K. M. Itoh, J. Appl. Phys. **96** 1754 (2004).
[28] B. J. Coomer, J. P. Goss, R. Jones, S Öberg, and P. R. Briddon, J. Phys.: Condens. Matter **13**, L1 (2001).
[29] Z. Ciechanowska, G. Davies, and E. C. Lightowlers, Solid State Commun. **49**, 427 (1984).
[30] K. L. Brower, *Phys. Rev.* B **14**, 872 (1976).
[31] D. Pierreux and A. Stesmans, Phys. Rev. B **68**, 193208 (2003).
[32] T. Mchedlidze and M. Suezawa, J. Phys.: Condens. Matter **15**, 3683 (2003).
[33] T. Mchedlidze and M. Suezawa, Physica B **340-342**, 682 (2003).
[34] A. Carvalho, R. Jones, J. Coutinho, V. J. B. Torres and P. R. Briddon, Phys. Rev. B **72**, 155208 (2005).
[35] S. K. Estreicher, M. Gharaibeh, P. A. Fedders, e P. Ordejón, *Phys. Rev. Lett.* **86**, 1247 (2001).
[36] J. F. Ziegler, J. P. Biersack, and U. Littmark, *The Stopping and Range of Ions in Solids* (Pergamon Press, New York, 1985).
[37] A. P. Knights, F. Malik, and P. G. Coleman, Applied Physics Letters **75**, 466 (1999).
[38] J. Tan, G. Davies, S. Hayama, and A. N. Larsen, Appl. Phys. Lett. **90**, 041910 (2007).
[39] A. S. Lyutovich, K. L. Lyutovich, V. P. Popov, and L. N. Safronov, Phys. Stat. Sol. (b) **129**, 313 (1985).
[40] G. S. Mitchard and T. C. McGill, Phys. Rev. B **25**, 5351 (1982).
[41] C. Hartwigsen, S. Goedecker, and J. Hutter, Phys. Rev. B **58**, 3641 (1998).
[42] P. R. Briddon, and R. Jones, Phys. Stat. Sol. (b) **217**, 131 (2000).
[43] H. J. Monkhorst, and J. D. Pack, Phys. Rev. B **13**, 5188 (1976).
[44] A. Balsas, J. Coutinho, V. J. B. Torres, P. R. Briddon, and M. Barroso, Phys. Rev. B **70**, 085201 (2004).
[45] J. C. Aubry, T. Tyliszczak, A. P. Hitchcock, J.-M. Baribeau, and T. E. Jackman, Phys. Rev. B **59**, 12872 (1999).
[46] From this point onwards, to simplify the notation, we refer Coomer's I_3 structure as I_3.
[47] J. P. Goss, M.J. Shaw, and P.R. Briddon, Topics in Applied Physics **104**, 69 (2007).
[48] A. Carvalho, J. Coutinho, R. Jones, J. Goss, M. Barroso, and P. R. Briddon, Phys. Rev. B **78**, 125208 (2008).
[49] J. Weber, and M. I. Alonso, Phys. Rev. B **40** 5683 (1989).